



CHORUS

This is the accepted manuscript made available via CHORUS. The article has been published as:

Superconducting phase of TiO_xTi thin films grown by molecular beam epitaxy

Yasemin Ozbek, Cooper Brooks, Xuanyi Zhang, Athby Al-Tawhid, Vladimir A. Stoica, Zhan Zhang, and Divine P. Kumah

Phys. Rev. Materials **6**, 064805 — Published 27 June 2022

DOI: [10.1103/PhysRevMaterials.6.064805](https://doi.org/10.1103/PhysRevMaterials.6.064805)

Superconducting Phase of Ti_xO_y Thin Films Grown by Molecular Beam Epitaxy

Yasemin Ozbek,¹ Cooper Brooks,¹ Xuanyi Zhang,¹ Athby Al-Tawhid,¹

Vladimir A. Stoica,² Zhan Zhang,³ and Divine P. Kumah^{1,*}

¹*Department of Physics, North Carolina State University, Raleigh, NC, 27695, USA*

²*Department of Materials Science and Engineering and Materials Research Institute, Pennsylvania State University, University Park, PA 16802, USA*

³*Advanced Photon Source, Lemont, IL 76019, USA*

(Dated: June 9, 2022)

We investigate the complex relationship between the growth conditions and the structural and transport properties of Ti_xO_y thin films grown by molecular beam epitaxy. Transport properties ranging from metallicity to superconductivity and insulating states are stabilized by effectively tuning the O/Ti ratio via the Ti flux rate and the O partial pressure, P_{O_x} , for films grown on (0001)- Al_2O_3 substrates at 850° C. A cubic $c - \text{TiO}_{1\pm\delta}$ buffer layer is formed for low O/Ti ratios while a corundum $\text{cr} - \text{Ti}_2\text{O}_3$ layer is formed under higher oxidizing conditions. Metallicity is observed for $c - \text{TiO}_{1-\delta}$ buffer layers. The superconducting $\gamma - \text{Ti}_3\text{O}_5$ Magnéli phase is found to nucleate on a $c - \text{TiO}_{1-\delta}$ buffer for intermediate P_{O_x} conditions and an insulator-superconducting transition is observed at 4.5 K ($T_C^{\text{onset}} = 6\text{K}$) for 85 nm thick films. Strain relaxation of the $\gamma - \text{Ti}_3\text{O}_5$ occurs with increasing film thickness and correlates with a thickness-dependent increase in T_C observed for Ti_xO_y thin films.

I. INTRODUCTION

The simple binary oxide, titanium oxide, Ti_xO_y , forms a wide range of polymorphs and Magnéli ($\text{Ti}_n\text{O}_{n-1}$) phases with properties ranging from insulating rutile and anatase TiO_2 , to corundum $\text{cr} - \text{Ti}_2\text{O}_3$ which undergoes a metal-insulator transition at 450 K, to superconducting cubic NaCl-type $c - \text{TiO}$ (bulk $T_C = 1\text{-}2\text{ K}$). [1–5] The ability to utilize the epitaxial stabilization of a given phase in thin films synthesised with atomic-layer control provides a route to tune the electronic properties of Ti_xO_y . [6–12] Recent reports of superconductivity in Ti_xO_y thin films as high as 11 K has sparked renewed interest in superconducting binary oxides. [13] The transition temperature, T_C has been reported to depend on the film thickness, [14, 15] oxygen stoichiometry [16, 17] and growth temperature [15]. The enhanced T_C in thin films was attributed to the formation of a high growth-temperature orthorhombic $o - \text{Ti}_2\text{O}_3$ phase [15] ($T_C = 8\text{ K}$), excess oxygen in $c - \text{TiO}_{1+\delta}$ films ($T_C = 7.4\text{ K}$) [6, 16], interfacial superconductivity at stoichiometric $c - \text{TiO}$ /non-stoichiometric $\text{TiO}_{1+\delta}$ interfaces in core-shell structures ($T_C = 11\text{ K}$) [13], and the epitaxial stabilization of the $\gamma - \text{Ti}_3\text{O}_5$ ($T_C = 7\text{ K}$) [18] Magnéli phase. Studies of mixed eutectic phases indicated a correlation between the coexistence of $c - \text{TiO}_{1+\delta}$, $\text{cr} - \text{Ti}_2\text{O}_3$ and $\gamma - \text{Ti}_3\text{O}_5$ phases with enhanced T_C hinting at the non-trivial role of interactions at interfaces between Ti_xO_y phases in enhancing T_C . [19] Thus, a critical step in understanding the enhanced transition temperature, T_C , in Ti_xO_y thin films involves elucidating the atomic-scale structure and composition of the system as a function of growth conditions (growth temperature, oxygen pressure, film thickness) using synthesis techniques which allow for the control of the film stoichiometry.

The relation between the transport properties and structural phases of Ti_xO_y was previously investigated for thin films grown by pulsed laser deposition (PLD) and molecular beam epitaxy (MBE) on (0001)-oriented $\alpha - \text{Al}_2\text{O}_3$. [6, 11, 16, 18–22] Figure 1 shows the lattice structures of the lattice planes of Ti_xO_y phases grown epitaxially on (0001)-oriented $\alpha - \text{Al}_2\text{O}_3$. A summary of reported phases and their superconducting T_C s is given in Table I. Li *et. al.* reported an orthorhombic $o - \text{Ti}_2\text{O}_3$ phase for films grown by PLD above 650° C as evidenced by high-resolution transmission electron microscopy (TEM), Raman spectroscopy and specular X-ray diffraction measurements (XRD). [11, 15] They observed a dependence of T_C on the film thickness of the $o - \text{Ti}_2\text{O}_3$ phase with a maximum T_C of 8 K for 168 nm thick films. [15] Low temperature growth (below 650 °C) led to the stabilization of the insulating bulk trigonal $\text{cr} - \text{Ti}_2\text{O}_3$ phase. Fan *et. al.* investigated the growth oxygen pressure dependence between 4.5×10^{-6} to 6.7×10^{-6} Torr for 80 nm thick films and found a suppression of superconductivity at high oxygen growth pressures. [16] The conclusion of a $c - \text{TiO}$ structure was based on the analysis of the film layers close to the substrate by TEM and XRD measurements. [6] It is important to note that while multiple structures have been proposed/observed, the T_C s are consistent with the reported thickness-dependence. [14, 15] Additionally, local TEM measurements indicated a

* dpkumah@ncsu.edu

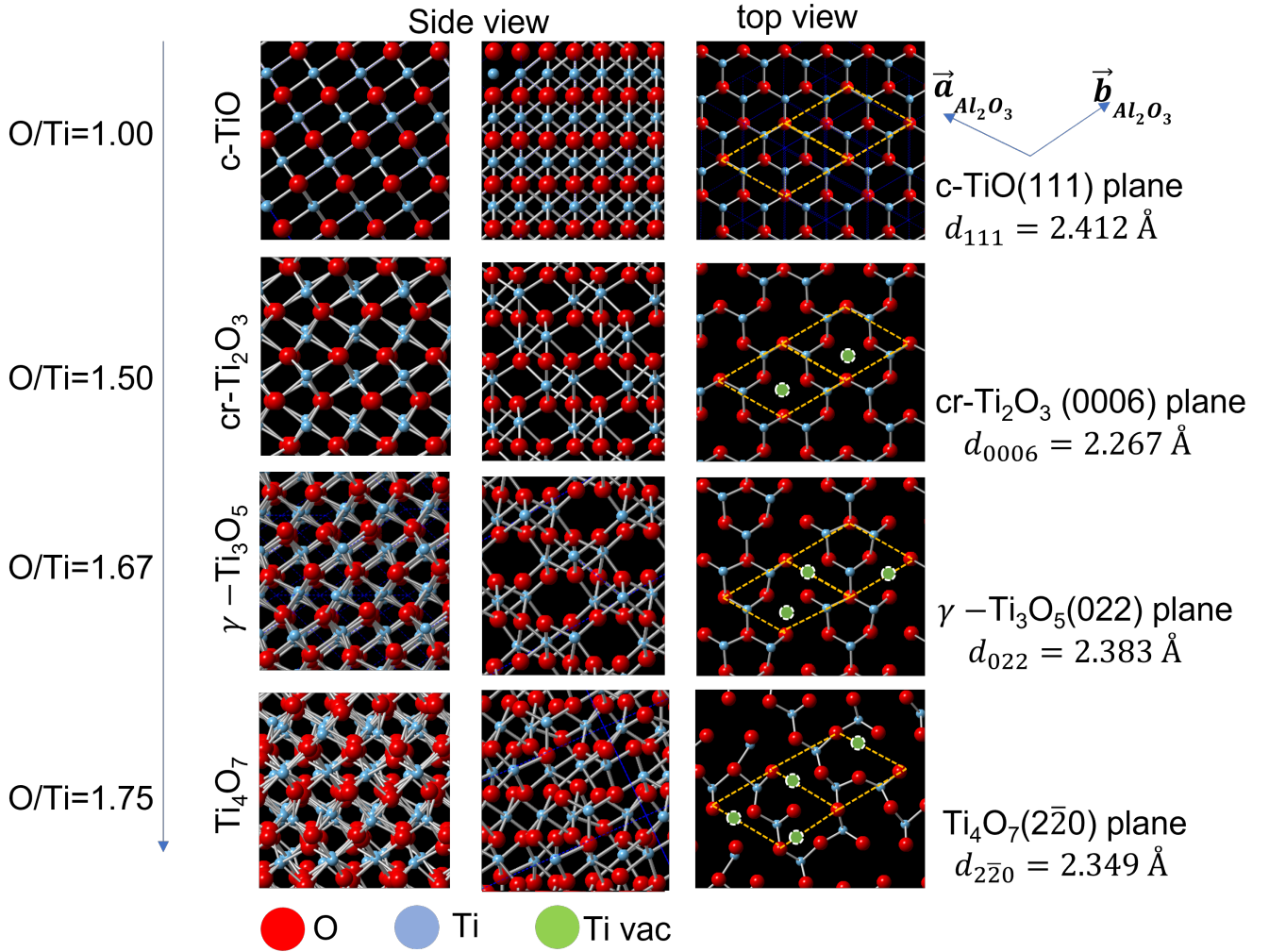


FIG. 1. Atomic structure of cubic c-TiO, corundum cr - Ti₂O₃, γ - Ti₃O₅ and Ti₄O₇ along projections in the α - Al₂O₃ [10 $\bar{1}$ 0] direction (left panel), [11 $\bar{2}$ 0] direction (middle panel) and the [0001] direction (right panel).

transitional c-TiO interface layer for o-Ti₂O₃. [15] A study of eutectic Ti_xO_y prepared by varying the growth and post-growth Ar annealing conditions showed a variation of T_C with the relative fractions of c-TiO, γ - Ti₃O₅ and cr - Ti₂O₃. Thus, the complexity of the system requires a systematic investigation of how specific growth conditions influence the relative fractions of the phases of Ti_xO_y and the resulting effect on the transport properties.

In this letter, we investigate the transport and structural properties of Ti_xO_y films grown by MBE to elucidate the effect of tuning the film stoichiometry and thickness on the superconducting properties of Ti_xO_y thin films. Here, we perform high-resolution synchrotron X-ray diffraction measurements on Ti_xO_y films grown on (0001)-oriented α - Al₂O₃ at 850 °C. The film stoichiometry is tuned by controlling the growth oxygen pressure, P_{O_x} , Ti flux rate, and film thickness. P_{O_x} is varied from 4×10^{-8} Torr to 1×10^{-6} Torr. Films grown at low oxygen partial pressures ($P_{O_x} \leq 1 \times 10^{-7}$ Torr) are found to be metallic with carrier concentrations ranging from $3 \times 10^{22} \text{ cm}^{-3}$ at 300 K to $6 \times 10^{21} \text{ cm}^{-3}$ at 10 K. Metallicity is correlated with the formation of oxygen-deficient c-TiO_{1- δ} . By tuning the P_{O_x} , the Ti flux rate and the film thickness, an insulating-superconducting transition is observed in 85 nm thick films which are characterized by a thin c-TiO_{1 \pm δ} interfacial buffer layer and the formation of the γ - Ti₃O₅ phase. Strain relaxation is observed in γ - Ti₃O₅ with increasing film thickness and correlates with a thickness-tuned T_C observed in Ti_xO_y films. [14, 15]

Substrate (Method)	Thickness	Structure	T_c
Al_2O_3 (PLD)	80 nm	$\text{TiO}_{1\pm\delta}$	7.4 K [6]
(Sintering)	bulk	$\text{TiO}_{1\pm\delta}$	5.5 K [22]
Al_2O_3 (PLD)	168 nm	$o\text{-Ti}_2\text{O}_3$	8 K [15]
Al_2O_3 (PLD)	120 nm	$o\text{-Ti}_2\text{O}_3$	I (no T_c) [11]
Al_2O_3 (PLD)	120 nm	$\gamma\text{-Ti}_3\text{O}_5$	7.1 [18]
LSAT, MgAl_2O_4 (PLD)	120 nm	Ti_4O_7	3.0 [18]
Al_2O_3 (PLD)	80 nm	$\text{TiO}_{1\pm\delta}$	1.4-6 K [16]
Al_2O_3 (PLD)	150 nm	$cr\text{-Ti}_2\text{O}_3$	I(no T_c) [20]

TABLE I. Summary of reported Ti_xO_y structures and superconducting transition temperatures, T_c . I refers to insulating phase.

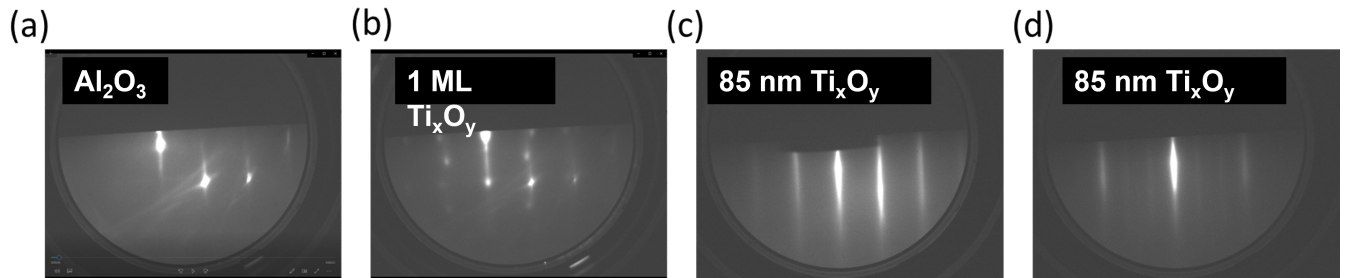


FIG. 2. Evolution of the surface RHEED pattern for the growth of 85 nm thick Ti_xO_y film on (0001)-oriented $\alpha\text{-Al}_2\text{O}_3$ at $P_{\text{O}_2} = 2 \times 10^{-7}$ Torr and a growth rate of 2.5 $\text{\AA}/\text{min}$ (Sample E). (a) Diffraction pattern of the initial Al_2O_3 surface (b) after 1 ML Ti_xO_y along the $[1120]$ azimuth, (c) after 85 nm along the $[1120]$ and (d) $[1010]$ directions.

II. RESULTS AND DISCUSSION

Ti_xO_y films with thicknesses 25-85 nm were grown by oxide MBE. Prior to growth, the Al_2O_3 substrates were annealed at 1100 $^\circ\text{C}$ in a tube furnace tube for 12 hours. Atomic force microscope images show smooth surfaces with atomic steps. The films were grown by deposition of Ti from an effusion cell under partial pressures of molecular oxygen ranging from 4×10^{-8} to 1×10^{-6} Torr at a substrate temperature of 850 $^\circ\text{C}$. The growth rates were determined from the Ti fluxes measured by a quartz crystal monitor and X-ray reflectivity measurements to be 1.3-2.5 $\text{\AA}/\text{min}$. The sample growth conditions are summarized in Table II. After growth, the films were cooled down at a rate of 25 $^\circ\text{C}/\text{min}$ from the deposition temperature to room temperature in vacuum.

Sample	Thickness	Ti flux ($\text{atoms}/\text{cm}^2\text{s}$)	rate	P_{O_x} (Torr)	Normalized $P_{\text{O}_x}/T_{i\text{rate}}$	Phase	Transport
A	25 nm	1.2×10^{13}		3×10^{-7}	2.9	$cr\text{-Ti}_2\text{O}_3$	I
B	25 nm	1.2×10^{13}		4×10^{-8}	0.4	$c\text{-TiO}_{1-\delta}$, $\gamma\text{-Ti}_3\text{O}_5$	M
C	25 nm	1.2×10^{13}		8×10^{-8}	0.8	$c\text{-TiO}_{1-\delta}$, $\gamma\text{-Ti}_3\text{O}_5$	M
D	45 nm	2.4×10^{13}		2×10^{-7}	1.0	$c\text{-TiO}_{1-\delta}$, $\gamma\text{-Ti}_3\text{O}_5$	M, SC
E	85 nm	2.4×10^{13}		2×10^{-7}	1.0	$c\text{-TiO}$, $\gamma\text{-Ti}_3\text{O}_5$	I, SC
F	80 nm	1.7×10^{13}		2×10^{-7}	1.4	$c\text{-TiO}/\gamma\text{-Ti}_3\text{O}_5$, $cr\text{-Ti}_2\text{O}_3$, Ti_4O_7	I, SC

TABLE II. Summary of growth conditions, film thickness and measured phases and transport properties of MBE-grown Ti_xO_y films on (0001)-oriented $\alpha\text{-Al}_2\text{O}_3$. I, M and SC refer to the insulating, metallic and superconducting phases, respectively. The $P_{\text{O}_x}/T_{i\text{rate}}$ are normalized to the values for the superconducting Sample E.

Figure 2(a) shows an *in-situ* reflection high energy electron diffraction (RHEED) image of the initial Al_2O_3 substrate surface prior to deposition of the Ti_xO_y films at $P_{\text{O}_x} = 2 \times 10^{-7}$ Torr. Figure 2(b) shows the RHEED pattern after the deposition of 1 ML of Ti_xO_y . Roughening and relaxation are evident from the spotty nature of the RHEED pattern and the development of streaks with a closer spacing than the diffraction from the substrate. A streaky 2D pattern

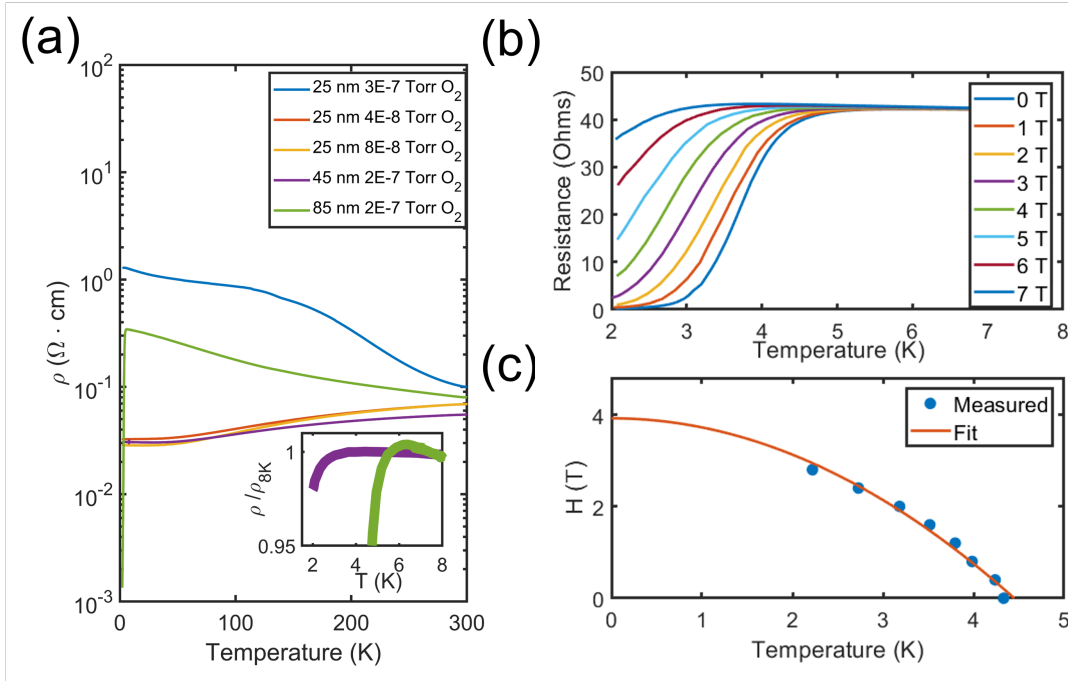


FIG. 3. (a) Comparison of sheet resistance for MBE-grown Ti_xO_y films as a function of growth oxygen pressure and film thickness. The inset shows the drop in resistivity at low temperatures for the superconducting samples (Samples D and E). (b) Resistivity as a function of magnetic field applied in-plane for 85 nm thick Ti_xO_y film (Sample E) grown at $P_{\text{O}_x} = 2 \times 10^{-7}$ Torr. (c) Relationship between critical magnetic field and T_C and the corresponding Werthamer-Helfand-Hohenberg (WHH) fit.

emerges after the 2nd ML and remains for the entire film growth. Figure 2(c) and 2(d) show the RHEED patterns after the growth of an 85 nm thick film along the $[11\bar{2}0]$ and $[10\bar{1}0]$ directions respectively. The narrow streaks are indicative of a smooth 2D surface. Along the $[10\bar{1}0]$ direction, a 3x reconstruction is observed. A comparison of the final RHEED patterns of Samples A-F is shown in Figure S1 of the supplemental materials.[23] Atomic force microscope images of the as-grown films (See Figure S2 of supplemental materials)[23] show atomically flat layers with step-like features identical to the substrate.

A. Transport Properties

The dependence of the transport properties on the film thickness and growth conditions is determined by comparing the resistivities of a series of Ti_xO_y films with thicknesses between 25 nm and 85 nm for $4 \times 10^{-8} \leq P_{\text{O}_x} \leq 3 \times 10^{-7}$ Torr in Figure 3(a). The transport measurements are performed in the Van der Pauw configuration using Au contacts deposited on the corners of $5\text{mm} \times 5\text{mm}$ samples. Films grown with $P_{\text{O}_x} \leq 1 \times 10^{-7}$ Torr are metallic for thicknesses less than 45 nm. Growth at higher oxygen pressures ($P_{\text{O}_x} \geq 3 \times 10^{-7}$ Torr) results in insulating transport properties.

At the intermediate growth pressure of $P_{\text{O}_x} = 2 \times 10^{-7}$ Torr, the transport properties depend on the film thickness and the Ti flux rate. The 45 nm film grown at $P_{\text{O}_x} = 2 \times 10^{-7}$ Torr (Sample D) is metallic and undergoes a metal-superconducting transition at ~ 3.7 K. The thicker 85 nm film (Sample E) is insulating below 300 K and transitions to a superconducting state at 4.5 K. The absence of superconductivity above 2 K for the 25 nm thick films, for the Ti flux rates investigated, is consistent with the thickness dependence of T_C observed for PLD grown films.[15] Films grown with $P_{\text{O}_x} > 8 \times 10^{-7}$ Torr are insulating due to the formation of TiO_2 as evidenced by X-ray diffraction measurements.

Superconductivity in the 85 nm film (Sample E) is confirmed by measuring the resistance as a function of a magnetic field, H applied parallel to the sample surface. Figure 3(b) shows the suppression of T_C for $0T < H < 7T$. The upper critical field $H_{C2}(T)$ is defined by a 90% drop in the normal state resistance. Figure 3(c) shows a plot of H_{C2} as a function of temperature. The results are fit to the Werthamer-Helfand-Hohenberg (WHH) equation $H_{C2}(T) = H_{C2}(0)[1 - (\frac{T}{T_C})^2]$. [24] From the fit, the upper critical field at 0 K, $H_{C2}(0)$ is determined to be 9.8 T. The coherence length, ξ , is determined to be 5.7 nm from the the Ginzburg-Landau superconducting coherence length

relation, $\xi = [(\hbar/2e)/(H_{c2}(0))]^{1/2}$. The measured coherence length is comparable to previous reports. [6, 16]

The insulating-superconducting transition has been previously observed in Ti_xO_y films[3, 14] and another 3D superconductor, $\text{BaPb}_{1-x}\text{Bi}_x\text{O}_3$ which also exhibits a strong dependence of T_C on the film thickness and the presence of multiple polymorphs (tetragonal and orthorhombic fractions of $\text{BaPb}_{1-x}\text{Bi}_x\text{O}_3$).[25] Thus, structural disorder arising from local fluctuations in oxygen content may enhance disorder leading to the insulator-superconductor transition.

B. XRD Structure

The relationship between the synthesis conditions, crystal structure, and the transport properties is determined by synchrotron XRD measurements at the 33ID beamline at the Advanced Photon Source. Figure 4(a) shows a specular scan around the substrate (0006) Bragg peak measured with an X-ray energy of 16 KeV ($\lambda = 0.774 \text{ \AA}$) for a series of Ti_xO_y samples. For Sample A grown with the highest $P_{O_x}/T_{i_{rate}}$ ratio, the main Bragg peak corresponds to the $c\text{-Ti}_2\text{O}_3$ phase. A second peak is observed corresponding to a slightly O-rich $c\text{-TiO}$ layer.

The diffraction intensities for the 25 nm metallic Ti_xO_y film (Sample B) comprise of a broad shoulder with lattice spacing $d=2.423 \text{ \AA}$ and a main peak with $d=2.375 \text{ \AA}$. The shoulder and main peaks correspond, respectively, to the (111) Bragg reflection of oxygen-deficient $c\text{-TiO}_{1-\delta}$ and the (022) Bragg peak of $\gamma\text{-Ti}_3\text{O}_5$ compressively strained to the buffer layer.

While weak insulating behavior has been reported for $c\text{-TiO}_{1+\delta}$, the observation of metallicity in Samples B and C arises from the stabilization of Ti-rich/oxygen poor $c\text{-TiO}_{1-\delta}$ due to the low growth oxygen pressures. For $0.05 \leq \delta \leq 0.2$, Hulm *et. al.* show metallicity for as-cast single-phase $c\text{-TiO}_{1-\delta}$ samples.[3] An expansion in the lattice parameter is expected for the oxygen deficient $c\text{-TiO}_{1-\delta}$,[3] hence, from fits to the 00L data, the broad shoulder at low L ($c_{measured}=4.19 \text{ \AA}$) is assigned to a $\sim 15 \text{ \AA}$ thick metallic $c\text{-TiO}_{1-\delta}$ layer which dominates the resistivity measurements in Figure 3(a). Annealing Sample B in flowing O_2 for 3 hours at $600 \text{ }^\circ\text{C}$ leads to the oxidation of both layers and a shift in the Bragg peaks to $d=2.324 \text{ \AA}$ corresponding to the formation of $c\text{-Ti}_2\text{O}_3$ and a metal-insulator transition.

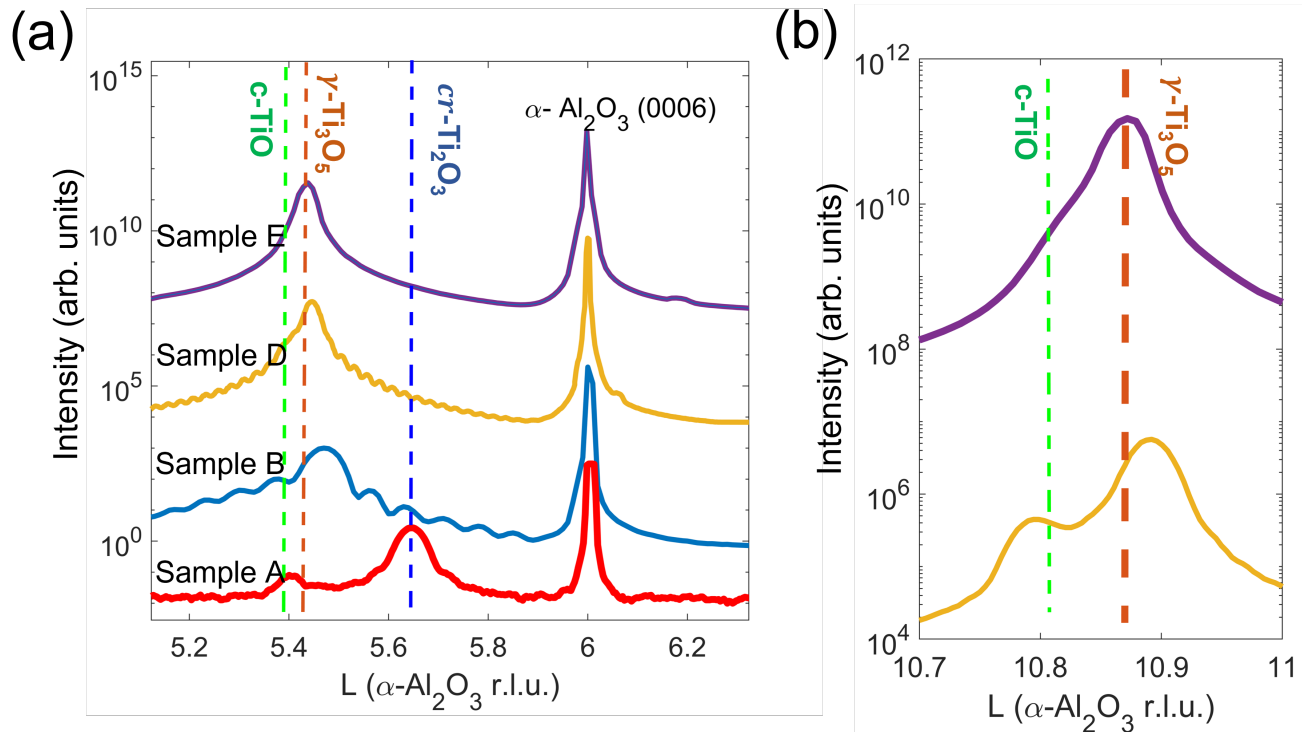


FIG. 4. (a) Comparison of specular X-ray diffraction around the $\alpha\text{-Al}_2\text{O}_3$ (0006) Bragg peak for a Samples A (25 nm, $P_{O_x} = 3 \times 10^{-7}$ Torr), B (25 nm, $P_{O_x} = 4 \times 10^{-8}$ Torr), D (45 nm, $P_{O_x} = 2 \times 10^{-7}$ Torr) and E (85 nm, $P_{O_x} = 2 \times 10^{-7}$ Torr) Ti_xO_y films grown by MBE. (b) Corresponding reflections for Sample D and E at higher q .

The 45 nm metallic Sample D also has a main peak at $d=2.385 \text{ \AA}$ corresponding to the (022) peak of $\gamma\text{-Ti}_3\text{O}_5$

and a shoulder with $d=2.4171 \text{ \AA}$ corresponding to slightly oxygen-deficient $c\text{-TiO}_{1-\delta}$. The metallicity observed for this sample is again, due to the metallic oxygen-deficient $c\text{-TiO}_{1-\delta}$ layer. Around 3.7 K, a decrease in the resistivity is observed (Figure 3(a) inset) due to the superconducting transition in the $\gamma\text{-Ti}_3\text{O}_5$ layer.[18]

The superconducting Sample E has a main Bragg peak at $d=2.388 \text{ \AA}$ corresponding to the (022) peak of relaxed $\gamma\text{-Ti}_3\text{O}_5$. Close to the (044) $\gamma\text{-Ti}_3\text{O}_5$ in Figure 4(b), we observe a shoulder at lower q which corresponds to the (222) reflection of cubic stoichiometric TiO ($c_{\text{measured}} = 4.167 \text{ \AA}$). The metallic phase is strongly suppressed, possibly, due to the longer deposition time which allows for complete oxidation of the $c\text{-TiO}$ buffer layer. The transport properties of the Sample E in Figure 3(a) are dominated by the superconducting relaxed $\gamma\text{-Ti}_3\text{O}_5$ phase.[17]

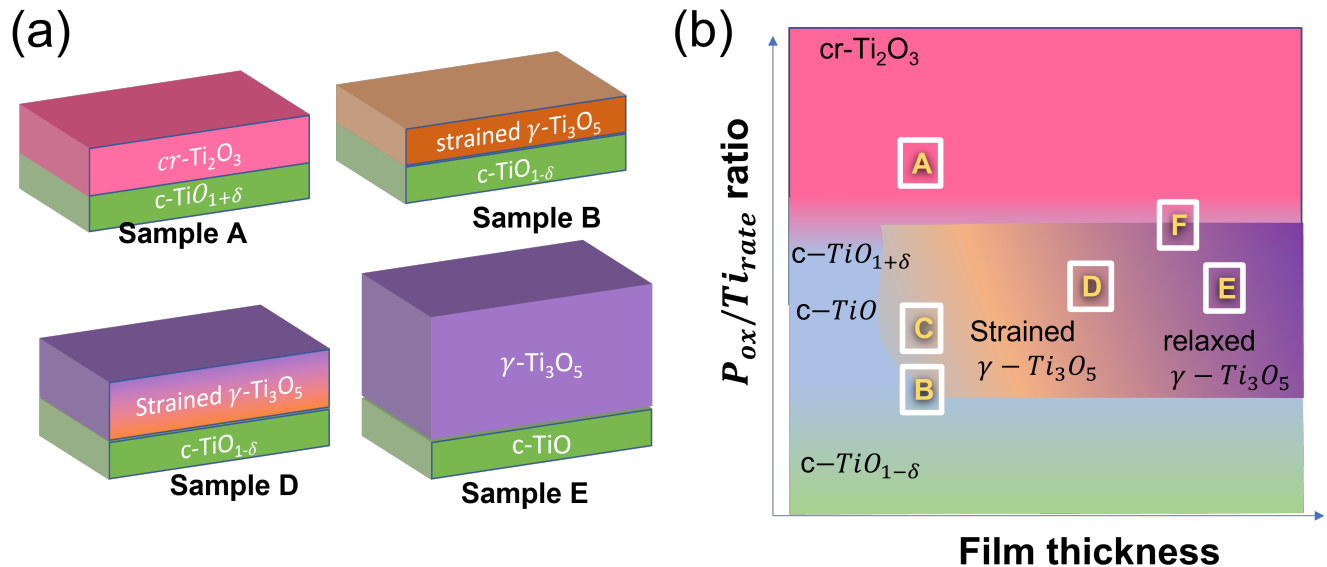


FIG. 5. (a) Schematic structures of samples A,B,D and E determined from X-ray diffraction measurements and (b) the corresponding phase diagram showing the relationship between the ratio of the growth oxygen pressure P_{ox} to the Ti flux rate and the film thickness.

Based on the X-ray diffraction measurements, the emergent picture of the structural profiles of the films under different growth conditions is summarized in Figure 5. Oxygen-poor growth of Ti_xO_y on (0001)-oriented $\alpha\text{-Al}_2\text{O}_3$ at high growth temperatures leads to the formation of a thin (111)-oriented cubic $\text{TiO}_{1-\delta}$ metallic buffer layer. As the film thickness increases, if the oxygen pressure is sufficiently high, the structure transforms into the Magnéli $\gamma\text{-Ti}_3\text{O}_5$ phase. The $\gamma\text{-Ti}_3\text{O}_5$ is initially strained to the buffer layer and the strain is relaxed as the film thickness is increased. Since pressure is known to suppress superconductivity in Ti_xO_y , [6] this picture is consistent with the observed increase in T_C with increasing film thickness.[15, 17]

C. Phase segregation in Ti_xO_y

The transport and structural results indicate a strong correlation between the growth conditions and film thickness on the physical and structural properties of the Ti_xO_y films. Stoichiometric $c\text{-TiO}$ has an NaCl structure with lattice constant $c=4.177 \text{ \AA}$. The NaCl structure is stable for oxygen concentrations ranging from 0.8 to 1.3 with T_C increasing from 0.5 K to 1 K for bulk $c\text{-TiO}_x$. [3, 5, 8, 26] The tendency of Ti_xO_y to form Magnéli phases and related polymorphs of the form $\text{Ti}_n\text{O}_{2n-1}$ suggests that the oxygen stoichiometry and the growth conditions strongly influence the structure and physical properties of the thin films.

To further investigate the delicate balance between film stoichiometry and the transport properties of the Ti_xO_y system, we consider the structural properties of an eutectic film formed by growing at a reduced Ti rate with the oxygen pressure of 2×10^{-7} Torr. The slight increase in the O/Ti ratio is expected to allow for the thermodynamic stabilization of oxygen-rich Ti_xO_y phases such as $cr\text{-Ti}_2\text{O}_3$.

The initial RHEED images for the sample grown at the lower Ti rate shows diffraction spots indicative of surface roughening, however, the final RHEED image in Figure 6(a) shows well defined 2D streaks after the growth of 80 nm. Figure 6(b) shows an optical image of the as-grown film. Clear dark and bright regions are observed indicating

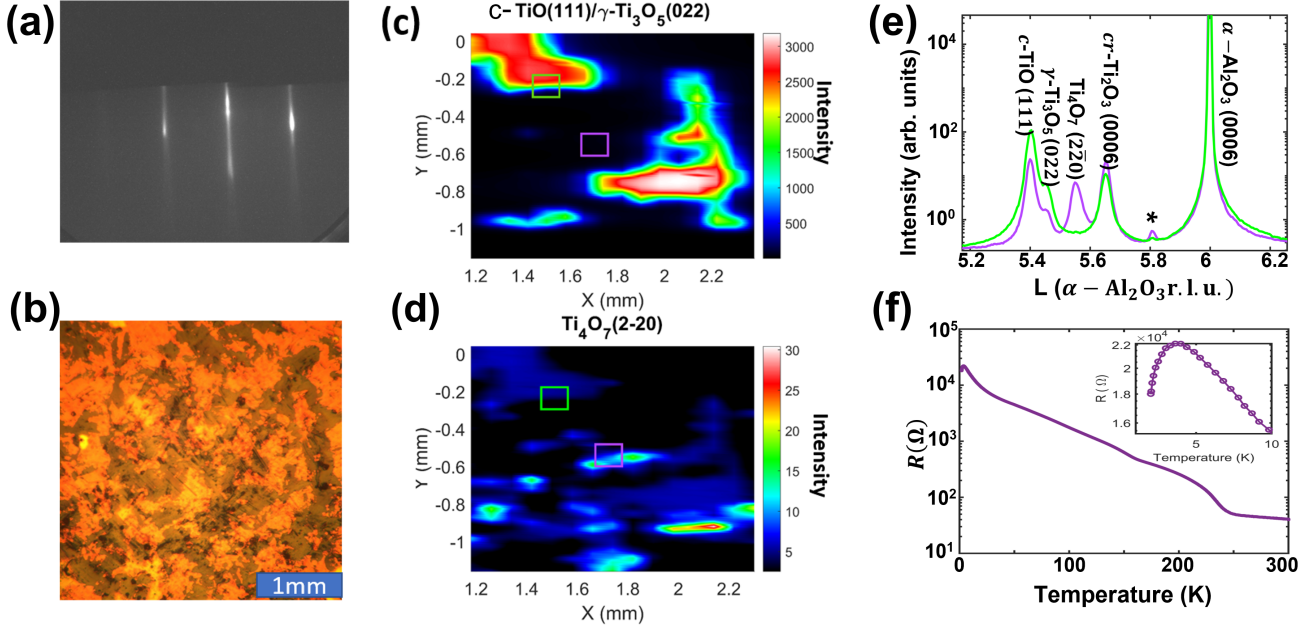


FIG. 6. Structural and transport properties of a 80 nm thick Ti_xO_y film grown at Ti flux rate of $1.8 \text{ \AA}/\text{min}$ in $P_{\text{O}_2} = 2 \times 10^{-7}$ Torr (Sample F). (a) Reflection high energy diffraction for 80 nm Ti_xO_y on (0001)-oriented Al_2O_3 . (b) Optical micrograph of film indicating structural domains. High-resolution synchrotron X-ray diffraction raster maps around Bragg peaks observed at diffraction conditions fixed for (c) $c\text{-TiO}$ (111) Bragg peak and (d) Ti_4O_7 ($2\bar{2}0$) Bragg peak indicating structural phase separation. (e) Specular diffraction along the substrate 00L direction at different points on the sample. (f) Resistance versus temperature. The inset shows the superconducting transition at low temperature.

macroscopic phase separation. These variations are not observed for the uniform films previously discussed (Figure S3 of supplemental materials)[23]. To determine the differences in the structure of the observed phases, we perform micro-diffraction experiments at the Advanced Photon source where the X-ray beam is focused to a $20\mu\text{m} \times 40\mu\text{m}$ spot size using a KirkpatrickBaez mirror. Figure 6(c) and 6(d) shows diffraction intensity maps with the diffraction conditions fixed at the $c\text{-TiO}$ (111) Bragg reflection and the Ti_4O_7 ($2\bar{2}0$) reflection. The maps show that the two phases are not uniformly distributed throughout the sample. Figure 6(e) shows (00L) scans at locations close to the $c\text{-TiO}$ phase and the Ti_4O_7 domain. The scans show that the intensity of the Ti_4O_7 is suppressed in regions of the film with increased fractions of the $c\text{-TiO}$ and $\gamma\text{-Ti}_3\text{O}_5$ phase. At both locations surveyed in Figure 6(e), a $cr\text{-Ti}_2\text{O}_3$ peak is present indicating that the $c\text{-TiO}/\gamma\text{-Ti}_3\text{O}_5$ and Ti_4O_7 grains are located in a matrix of the insulating $cr\text{-Ti}_2\text{O}_3$ phase (The regions with 0 intensity in Figure 6(c) and (d)). The Ti_4O_7 grains have lateral dimensions on the order of $100 \mu\text{m}$ while the $c\text{-TiO}/\gamma\text{-Ti}_3\text{O}_5$ grains are an order of magnitude larger in dimensions. An additional peak indicated by the asterisk (*) at $L \approx 5.8$ r.l.u. ($d=2.18 \text{ \AA}$) suggests the presence of a small fraction of rutile TiO_2 .

The transport properties of the eutectic sample is shown in Figure 6(f). The multiple electronic transitions are consistent with the coexistence of multiple structural phases. Transitions in the resistivity are observed at 250 K and 150 K which are consistent with reported transitions for $cr\text{-Ti}_2\text{O}_3$ [19] and Ti_4O_7 [18]. The resistivity drops at 3 K is indicative of a superconducting transition expected for either Ti_4O_7 or $\gamma\text{-Ti}_3\text{O}_5$, however, no zero-resistant state is observed at the instruments minimum temperature of 2 K.

III. CONCLUSION

In conclusion, we have used a combination of high-resolution synchrotron X-ray diffraction mapping and temperature-dependent transport to investigate the correlation between film thickness, phase separation and superconductivity in Ti_xO_y films grown on (0001)-oriented $\alpha\text{-Al}_2\text{O}_3$. The films with thicknesses ranging from 25 to 85 nm are grown by MBE where the oxygen stoichiometry of the films is tuned by the oxygen partial pressure and the Ti flux rate during growth. The transport properties are correlated with the $P_{\text{ox}}/\text{Ti}_{\text{rate}}$ ratio and thickness-dependent strain relaxation. A metallic $c\text{-TiO}_{1-\delta}$ buffer layer is formed for films grown under oxygen-poor conditions. A superconducting Magnélli

$\gamma - \text{Ti}_3\text{O}_5$ layer nucleates on the buffer layer. Strain-relaxation occurs as the film thickness increases and correlates with a thickness-dependent increase in T_C . As the P_{ox}/Ti flux ratio increases, the buffer composition transitions to an insulating $\alpha\text{-Ti}_2\text{O}_3$ phase. A mixed-phase structure is formed for P_{ox}/Ti flux ratios close to the $\alpha\text{-TiO}/\alpha\text{-Ti}_2\text{O}_3$ phase boundary. These results suggest that the thickness-dependence of T_C in Ti_xO_y is related to a complex interplay between, strain and the nucleation kinetics of Ti_xO_y phases and polymorphs. Thus, a complete elucidation of phase formation and phase separation and the electronic and structural interactions at inter-phase boundaries will allow for understanding and enhancing T_C in atomically-thin Ti_xO_y layers.

ACKNOWLEDGMENTS

The authors acknowledge financial support by the US National Science Foundation under Grant No. NSF DMR-1751455. V.A.S. was supported by the US Department of Energy, Office of Science, Basic Energy Sciences under award number DE-SC-0012375. This work was performed in part at the Analytical Instrumentation Facility (AIF) at North Carolina State University, which is supported by the State of North Carolina and the National Science Foundation (award number ECCS-2025064). This work made use of instrumentation at AIF acquired with support from the National Science Foundation (DMR-1726294). The AIF is a member of the North Carolina Research Triangle Nanotechnology Network (RTNN), a site in the National Nanotechnology Coordinated Infrastructure (NNCI). Use of the Advanced Photon Source was supported by the U.S. Department of Energy, Office of Science, Office of Basic Energy Sciences, under Contract No. DE-AC02-06CH11357.

IV. DATA AVAILABILITY STATEMENT

The data that support the findings of this study are available from the corresponding author upon reasonable request.

-
- [1] N. Doyle, J. Hulm, C. Jones, R. Miller, and A. Taylor, Vacancies and superconductivity in titanium monoxide, *Physics Letters A* **26**, 604 (1968).
 - [2] H. Iwasaki, N. F. Bright, and J. Rowland, The polymorphism of the oxide Ti_3O_5 , *Journal of the Less Common Metals* **17**, 99 (1969).
 - [3] J. Hulm, C. Jones, R. Hein, and J. Gibson, Superconductivity in the TiO and NbO systems, *Journal of Low Temperature Physics* **7**, 291 (1972).
 - [4] D. McLachlan, New models for the positive and negative temperature coefficients of resistivity for $\text{TiO}_{0.80-1.23}$ metallic oxides, *Physical Review B* **25**, 2285 (1982).
 - [5] T. Reed, M. Banus, M. Sjöstrand, and P. Keesom, Superconductivity in Cubic and Monoclinic “TiO”, *Journal of Applied Physics* **43**, 2478 (1972).
 - [6] C. Zhang, F. Hao, G. Gao, X. Liu, C. Ma, Y. Lin, Y. Yin, and X. Li, Enhanced superconductivity in TiO epitaxial thin films, *npj Quantum Materials* **2**, 2 (2017).
 - [7] T. Wagner and M. Agarwal, Growth and Structure of Ti_2O_3 and TiO_2 Thin Films on (0001) $\alpha\text{-Al}_2\text{O}_3$ Substrates, *MRS Online Proceedings Library* **472**, 81 (1997).
 - [8] F. Li, Y. Zou, M.-G. Han, K. Foyevtsova, H. Shin, S. Lee, C. Liu, K. Shin, S. D. Albright, R. Sutarto, *et al.*, Single-crystalline epitaxial TiO film: A metal and superconductor, similar to Ti metal, *Science Advances* **7**, eabd4248 (2021).
 - [9] K. B. Alexander, F. J. Walker, R. A. McKee, and F. A. List III, $\text{TiOx}/\text{Al}_2\text{O}_3$ multilayer ceramic thin films, *Journal of the American Ceramic Society* **73**, 1737 (1990).
 - [10] Y. Li, Z. G. Yu, L. Wang, Y. Weng, C. S. Tang, X. Yin, K. Han, H. Wu, X. Yu, L. M. Wong, *et al.*, Electronic-reconstruction-enhanced hydrogen evolution catalysis in oxide polymorphs, *Nature Communications* **10**, 1 (2019).
 - [11] Y. Li, Y. Weng, X. Yin, X. Yu, S. S. Kumar, N. Wehbe, H. Wu, H. N. Alshareef, S. J. Pennycook, M. B. Breese, *et al.*, Orthorhombic Ti_2O_3 : A Polymorph-Dependent Narrow-Bandgap Ferromagnetic Oxide, *Advanced Functional Materials* **28**, 1705657 (2018).
 - [12] K. Yoshimatsu, N. Hasegawa, Y. Nambu, Y. Ishii, Y. Wakabayashi, and H. Kumigashira, Metallic ground states of undoped Ti_2O_3 films induced by elongated c-axis lattice constant, *Scientific Reports* **10**, 1 (2020).
 - [13] J. Xu, D. Wang, H. Yao, K. Bu, J. Pan, J. He, F. Xu, Z. Hong, X. Chen, and F. Huang, Nano Titanium Monoxide Crystals and Unusual Superconductivity at 11 K, *Advanced Materials* **30**, 1706240 (2018).
 - [14] C. Zhang, Y. Fan, Q. Chen, T. Wang, X. Liu, Q. Li, Y. Yin, and X. Li, Quantum Griffiths singularities in TiO superconducting thin films with insulating normal states, *NPG Asia Materials* **11**, 1 (2019).
 - [15] Y. Li, Y. Weng, J. Zhang, J. Ding, Y. Zhu, Q. Wang, Y. Yang, Y. Cheng, Q. Zhang, P. Li, *et al.*, Observation of superconductivity in structure-selected Ti_2O_3 thin films, *NPG Asia Materials* **10**, 522532 (2018).

- [16] Y. Fan, C. Ma, T. Wang, C. Zhang, Q. Chen, X. Liu, Z. Wang, Q. Li, Y. Yin, and X. Li, Quantum superconductor-insulator transition in titanium monoxide thin films with a wide range of oxygen contents, *Physical Review B* **98**, 064501 (2018).
- [17] Y. Fan, C. Zhang, X. Liu, Y. Lin, G. Gao, C. Ma, Y. Yin, and X. Li, Structure and transport properties of titanium oxide (Ti_2O , $TiO_{1+\delta}$, and Ti_3O_5) thin films, *Journal of Alloys and Compounds* **786**, 607 (2019).
- [18] K. Yoshimatsu, O. Sakata, and A. Ohtomo, Superconductivity in Ti_4O_7 and $\gamma - Ti_3O_5$ films, *Scientific Reports* **7**, 12544 (2017).
- [19] H. Kurokawa, K. Yoshimatsu, O. Sakata, and A. Ohtomo, Effects of phase fraction on superconductivity of low-valence eutectic titanate films, *Journal of Applied Physics* **122**, 055302 (2017).
- [20] K. Yoshimatsu, H. Kurokawa, K. Horiba, H. Kumigashira, and A. Ohtomo, Large anisotropy in conductivity of Ti_2O_3 films, *APL Materials* **6**, 101101 (2018).
- [21] C. Zhang, F. Hao, X. Liu, Y. Fan, T. Wang, Y. Yin, and X. Li, Quasi-two-dimensional vortex-glass transition and the critical current density in TiO epitaxial thin films, *Superconductor Science and Technology* **31**, 015016 (2017).
- [22] D. Wang, C. Huang, J. He, X. Che, H. Zhang, and F. Huang, Enhanced superconductivity in rock-salt TiO, *ACS Omega* **2**, 1036 (2017).
- [23] Supplemental Materials, .
- [24] N. Werthamer, E. Helfand, and P. Hohenberg, Temperature and purity dependence of the superconducting critical field, H_{c2} . III. Electron spin and spin-orbit effects, *Physical Review* **147**, 295 (1966).
- [25] D. T. Harris, N. Campbell, R. Uecker, M. Brützmam, D. G. Schlom, A. Levchenko, M. S. Rzchowski, and C.-B. Eom, Superconductivity-localization interplay and fluctuation magnetoresistance in epitaxial $BaPb_{1-x}Bi_xO_3$ thin films, *Physical Review Materials* **2**, 041801 (2018).
- [26] M. Banus, T. Reed, and A. Strauss, Electrical and magnetic properties of TiO and VO, *Physical Review B* **5**, 2775 (1972).